Original Article

Diabetes Enhances mRNA Levels of Proapoptotic Genes and Caspase Activity, Which Contribute to Impaired Healing

Hesham A. Al-Mashat, Suneel Kandru, Rongkun Liu, Yugal Behl, Tesfahun Desta, and Dana T. Graves

We previously reported that after a bacteria-induced wound in the scalp, type 2 diabetic (*db/db*) mice had higher levels of apoptosis of fibroblasts and bone-lining cells that are critical for healing compared with normoglycemic controls. To investigate mechanisms by which this might occur, RNA profiling and caspase activity was measured after inoculation of *Porphyromonas gingivalis*. Diabetes caused a more than twofold induction of 71 genes that directly or indirectly regulate apoptosis and significantly enhanced caspase-8, -9, and -3 activity. The functional significance of diabetes-induced apoptosis was studied by treating diabetic mice with a pancaspase inhibitor, z-VAD-fmk (*N*-benzyloxycarbonyl-Val-Ala-Asp-fluoromethylketone). Inhibiting apoptosis significantly improved several parameters of healing, including fibroblast density, enhanced mRNA levels of collagen I and III, and increased matrix formation. Improvements were also noted in bone, with an increase in the number of bone-lining cells and new bone formation. Thus, diabetes-enhanced apoptosis represents an important mechanism through which healing is impaired, and this can be explained, in part, by diabetes-increased expression of proapoptotic genes and caspase activity. *Diabetes* 55: 487–495, 2006

Diabetes affects >18 million Americans and causes significant morbidity and mortality (1). Diabetes complications that are debilitating include poor wound healing (2). The impaired healing affects the resolution of both acute and chronic wounds (3), which represent a significant health care burden in the U.S. As an example, ulcerations of the lower extremities, which heal poorly in diabetic patients, are a significant cause of hospitalization and are usually the first step in limb amputation (4). Of the 18 million people in the U.S. with diabetes, 20% will at some point develop ulcers that heal poorly (5,6).

Healing of wounds in diabetes is characterized by delays in the repair process as well as a decrease in the tensile strength of healing wounds (3,7). Deficiencies in fibroblast numbers have been reported to represent an important aspect of delayed wound healing in diabetes (8–10). It has been suggested that aberrant growth factor expression, altered inflammatory responses, or enhanced glycosylation of proteins may be involved (8,11,12). Alternatively, enhanced apoptosis may decrease fibroblast numbers, which could contribute to impaired diabetic healing (13). Whatever the cause, the generation and maintenance of a sufficient number of fibroblasts to participate in wound repair may be particularly important in diabetes.

Humans with type 1 diabetes have impaired osseous healing (14). That this may be caused by reduced bone formation is supported by findings that serum osteocalcin levels are significantly lower in type 1 diabetic patients (15), and there is a reduction in osteoblast numbers and function (16–18). In type 2 diabetes, there is evidence of diminished bone formation, increased risk of fracture, and impaired healing, but the mechanisms are not well established (19–21).

We previously reported that after inoculation of bacteria in the scalp, there is a bacteria-induced injury that is self-limited in nature and that demonstrates formation of an inflammatory infiltrate consisting largely of polymorphonuclear leukocytes on day 1, destruction of connective tissue matrix and bone resorption on days 3–5, initial healing of soft tissue on day 5, and peak healing of connective tissue and bone on day 8 (22,23). In the diabetic compared with normoglycemic group, there is impaired healing of connective tissue and bone and enhanced apoptosis of matrix-producing cells.

The current study was undertaken to examine the role of apoptosis in the healing response of connective tissue and bone to a bacteria-induced injury. This was accomplished by quantitative measurements of repair in *db/db* type 2 diabetic mice and their normoglycemic littermates. The functional role of apoptosis in the repair process was established using a pancaspase inhibitor. To better understand mechanisms by which diabetes may modulate the apoptotic process, mRNA profiling of genes that directly or indirectly affect apoptosis was undertaken, as were measurements of diabetes-enhanced caspase activity.

RESEARCH DESIGN AND METHODS

Genetically type 2 diabetic C57BL/KsJ-lepr$^{-/-}$ (*db/db*) mice and their normoglycemic littermates C57BL/KsJ-lepr$^{-/+}$ (*db/+*) mice were purchased from The Jackson Laboratory (Bar Harbor, ME). *db/db* mice developed diabetes at ~7–8 weeks of age and had fasting serum glucose levels >250 mg/dl for a minimum 20 days before the experiments were started. The glucose levels during the experimental period were typically 400–450 mg/dl in the *db/db*

From the Department of Periodontology and Oral Biology, Boston University School of Dental Medicine, Boston, Massachusetts.

Address correspondence and reprint requests to Dana T. Graves, Boston University School of Dental Medicine, W-202D, 700 Albany St., Boston, MA 02118. E-mail: dgraves@bu.edu.

Received for publication 12 September 2005 and accepted in revised form 2 November 2005.

Additional information for this article can be found in an online appendix at http://diabetes.diabetesjournals.org.

AFC, 7-amino-4-trifluoromethyl coumarin; TNF-α, tumor necrosis factor-α; TUNEL, transferase-mediated dUTP nick-end labeling.

TABLE 1
Direct intracellular regulators of apoptosis and transcription factors

Name	Array 1	Array 2	Mean fold difference	Description
Direct intracellular regulators of apoptosis				
Proapoptotic				
Dlgap3	6.1	7.2	6.7	Discs, large (*Drosophila*) homolog-associated protein 3
Casp9	7.1	5.5	6.3	Caspase 9, apoptosis-related cysteine protease
STK4	3.8	7.5	5.6	Serine/threonine kinase 4
Cias1	5.2	4.9	5.0	Cold autoinflammatory syndrome 1
Jmy	4.1	4.4	4.2	Junction-mediating and regulatory protein
Diablo	2.6	4.8	3.7	Diablo homolog (*Drosophila*)
Wwox	2.8	3.5	3.2	WW domain containing oxidoreductase
CdKn1a	2.7	3.3	3.0	Cyclin-dependent kinase inhibitor 1A (P21)
DAPK3	3.0	2.6	2.8	Death-associated protein kinase 3
Trim35	2.0	3.5	2.8	Tripartite motif–containing 35
Cflar	2.4	3.0	2.7	CASP8 and FADD-like apoptosis regulator
BCL-X	2.3	3.1	2.7	Apoptosis regulator bcl-xL
Bcl2l-11	3.0	2.3	2.6	BCL2-like 11 (apoptosis facilitator)
Casp3	2.2	2.4	2.3	Caspase 3, apoptosis-related cysteine protease
Bcl2l-10	1.8	2.5	2.2	BCL2-like 10 (apoptosis facilitator)
CARD4	2.0	2.1	2.0	Caspase recruitment domain family, member 4
Tia1	1.7	2.2	2.0	TIA1 cytotoxic granule-associated RNA-binding protein
BOK	2.2	1.7	2.0	BCL2-related ovarian killer
Antiapoptotic				
Birc7	6.9	6.2	6.5	Baculoviral IAP repeat–containing 7 (livin)
BNIP2	2.9	3.5	3.2	BCL2/adenovirus E1B 19 kDa–interacting protein 2
Bcl2	2.7	3.5	3.1	B-cell CLL/lymphoma 2
Birc3	2.1	2.7	2.4	Baculoviral IAP repeat–containing 3
Api5	2.8	2.0	2.4	Apoptosis inhibitor 5
SON	2.1	1.9	2.0	SON DNA-binding protein
NOL3	1.7	2.2	2.0	Nucleolar protein 3 (apoptosis repressor with CARD domain)
Birc4	0.3	0.4	0.4	Baculoviral IAP repeat–containing 4
Transcription factors				
Proapoptotic				
Ddit3	6.4	3.6	5.0	DNA-damage inducible transcript 3
Foxo3	3.9	3.2	3.6	Forkhead box O3
Mybl2	1.8	4.7	3.2	v-myb myeloblastosis viral oncogene homolog
E2f2	2.4	4.1	3.2	E2F transcription factor 2
Brca1	2.2	3.7	3.0	Breast cancer 1
Plagl-1	2.4	3.0	2.7	Pleiomorphic adenoma gene-like 1
Plagl-2	2.3	2.3	2.3	Pleiomorphic adenoma gene-like 2
Mitf	1.8	2.4	2.1	Microphthalmia-associated transcription factor
2F1	2.4	1.8	2.1	E2F transcription factor 1
Antiapoptotic				
Nkx3-1	2.3	6.2	4.2	NK3 transcription factor related, locus 1
p53	0.4	0.3	0.4	Cellular tumor antigen p53

mice and 100–150 mg/dl in the normoglycemic controls. All animal procedures were approved by the institutional animal care and use committee at Boston University Medical Center.

Inoculation of bacteria. *Porphyromonas gingivalis* was used to induce injury of connective tissue and bone based on its capacity to stimulate tissue loss in humans and in animal models (24,25). Broth-grown *P. gingivalis* strain 381 at log phase growth was fixed with 1% paraformaldehyde for 6 h. After mice were anesthetized with an injection of ketamine (80 mg/kg) and xylazine (10 mg/kg), 5×10^8 bacteria were inoculated at the midline of the scalp between the ears. This produces an inflammatory response, destruction of connective tissue, bone resorption, and a healing response that peaks in both diabetic and normoglycemic mice on day 8, as we have previously described (22,23). Mice were killed at 5 and 8 days after inoculation, and at no point did mice die from inoculation. There were six mice for each group at each data point ($n = 6$). The scalp and associated calvaria were prepared for histological sections. In some experiments the scalp was dissected free, snap-frozen in liquid nitrogen, pulverized, and protein or RNA extracted.

RNA profiling. Total RNA was isolated by Trizol reagent followed by RNeasy clean up (Qiagen, Valencia, CA). For each group, *db/db* or *db*/+, there were eight mice. The integrity, purity, and quantity of the samples were examined by agarose gel electrophoresis and by optical density readings (A_{260}/A_{280}), which were within the range of 1.9–2.1. The RNA levels were examined using a Mouse Genome 430 2.0 array (Affymetrix, Santa Clara, CA). Apoptosis-related genes were selected from the array data, using PathwayAssist software (Iobion, La Jolla, CA). All steps in microarray probe preparation, hybridization, and reading of fluorescent intensity was carried out by the Harvard-Forsyth Collaborative Microarray Core (Cambridge, MA). Two separate arrays were carried out each for normoglycemic and diabetic mice. The values for each gene were established and normalized using a probe logarithmic intensity error estimate (PLIER; Affymetrix). To be considered as modulated by diabetes, the intensity values were at least 1.7-fold different for each of the diabetic arrays compared with the mean of the normoglycemic group, and the mean of the diabetic group had to be at least 2.0-fold different compared with the mean of the normoglycemic group. For selected genes RNA was isolated from a separate set of eight *db/db* or eight *db*/+ mice, and the results were confirmed by real-time PCR. Taqman primer and probe sets for murine tumor necrosis factor-α (TNF-α), caspase-3, caspase-9, FADD (Fas-associating protein with death domain), Foxo1 (forkhead box 1), and Fas were purchased from Applied Biosystems (Foster City, CA). Results were normalized with an 18S ribosomal primer and probe set (Applied Biosystems). Each amplification

TABLE 2
Intercellular signaling

Name	Array 1	Array 2	Mean fold difference	Description
Proapoptotic				
CD30L	5.3	7.5	6.4	TNF (ligand) superfamily, member 8
IL-l7	2.7	6.8	4.8	Interleukin-17
SPP1	4.8	4.8	4.8	Secreted phosphoprotein 1 (osteopontin)
TRAIL	3.9	5.5	4.7	TNF (ligand) superfamily, member 10
GRAP2	2.6	5.4	4.0	GRB2-related adaptor protein 2
INS II	2.3	3.8	3.1	Insulin II
TNFsf7	2.3	3.5	2.9	TNF (ligand) superfamily, member 7
TNF	2.4	3.3	2.9	TNF
Nos1	2.7	2.7	2.7	Nitric oxide synthase 1 (neuronal)
LTα	1.8	3.4	2.6	Lymphotoxin-α (TNF-β)
BDNF	2.4	2.5	2.5	Brain-derived neurotrophic factor
Angptl-4	2.0	2.2	2.1	Angiopoietin-like 4
InhβA	1.9	2.3	2.1	Inhibin β-A chain precursor
Antiapoptotic				
TGFB1	0.3	0.6	0.5	Transforming growth factor-β1 precursor

was performed three times with duplicate specimens and the results from the replicates combined to establish statistical significance with Student's *t* test.

Treatment with caspase inhibitor. After inoculation of bacteria, animals were treated with the pancaspase inhibitor Z-VAD-FMK (Kamiya Biomedical). The inhibitor was applied starting 3 days after inoculation of bacteria (so as not to interfere with the early inflammatory phase) by intraperitoneal injection (2 mg/kg). Additional injections were performed daily thereafter until death. Control mice received the same volume of vehicle alone (0.2% DMSO in PBS).

Preparation of histological sections. After euthanasia, the head of each mouse was fixed for 72 h in cold 4% paraformaldehyde. Specimens were decalcified by incubation in cold Immunocal (Decal, Congers, NY) for ~2 weeks and then washed with Cal-Arrest (Decal). The scalp and underlying calvarial bone were kept intact, and paraffin-embedded sagittal sections were prepared at a thickness of 5 μm. All histological counts and measurements were from one examiner and were confirmed by an independent examiner. In all histological analysis, there were six mice per data point ($n = 6$). Student's *t* test was used to determine significant differences between the experimental and control groups.

Detection of apoptotic cells. Apoptotic cells were detected by an in situ transferase-mediated dUTP nick-end labeling (TUNEL) assay by means of a TACS 2 TdT-Blue label kit purchased from Trevigen (Gaithersburg, MD), following the manufacturer's instructions. This kit detects double-strand breaks in genomic DNA and identifies most stages of apoptosis. The number of fibroblastic apoptotic cells was counted at high magnification (1,000×) and were identified by their characteristic appearance in the connective tissue between the coronal and occipital sutures.

Histomorphometry. Van Gieson–stained sections were prepared as described previously (26) and were used to assess the area of new collagen formation at 400× magnification. Newly formed connective tissue matrix stains blue and was measured with computer-assisted image analysis. The total fibroblast number was counted at 1,000× magnification in the connective tissue between the coronal and occipital sutures in sections stained with

TABLE 3
Proapoptotic intracellular signaling and receptors

Array 1	Array 2	Mean fold difference	Name	Description
2.7	14.4	8.6	TRAILR2	Cytotoxic TRAIL receptor-2
2.7	14.4	8.6	TNFRsf10b	TNF receptor superfamily, member 10b
4.4	7.6	6.0	Psen1	Presenilin 1
5.5	3.8	4.7	IkBKγ	Inhibitor of γ light polypeptide gene enhancer in B-cells, kinase γ
2.6	5.7	4.1	TRAF6	TNF receptor–associated factor 6
3.6	3.2	3.4	MAPK14	Mitogen-activated protein kinase 14
2.9	3.8	3.3	Notch1	Notch homolog 1, translocation associated (*Drosophila*)
3.7	2.9	3.3	FAS	Apoptosis-mediating surface antigen Fas precursor (TNFRsf6)
2.4	4.2	3.3	TNFRsf11b	TNF receptor superfamily, member 11b (osteoprotegerin)
1.7	4.5	3.1	PTPN13	Protein tyrosine phosphatase, nonreceptor type 13
2.7	3.4	3.1	FADD	FADD protein
2.2	3.5	2.8	IGF1r	IGF-1 receptor precursor
1.8	3.7	2.7	Adra1a	Adrenergic α-1A receptor
2.2	3.2	2.7	PRKCα	Protein kinase C-α
2.9	2.4	2.7	PRKCζ	Protein kinase C-ζ
3.0	2.2	2.6	TNFRsf9	TNF receptor superfamily, member 9
2.9	2.2	2.5	MAPK8	Mitogen-activated protein kinase 8
2.4	2.6	2.5	MEK2	Mitogen-activated protein kinase kinase 2
2.4	2.4	2.4	MKK7	Mitogen-activated protein kinase kinase 7
1.8	2.9	2.4	TNFRsf1b	TNF receptor superfamily, member 1b
1.7	2.7	2.2	Apaf1	Apoptotic protease–activating factor
2.1	2.3	2.2	MAPK9	Protein kinase JNK2
2.4	1.8	2.1	Siva	CD27-binding (Siva) protein
2.3	1.8	2.0	TNFRsf5	TNF receptor superfamily, member 5

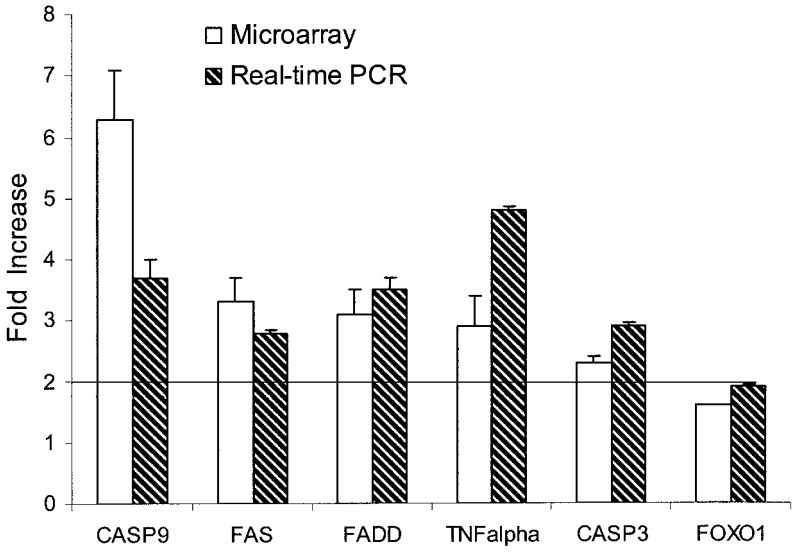

FIG. 1. Diabetes increases mRNA level of proapoptotic genes. Total RNA was isolated from the scalp 8 days after inoculation of *P. gingivalis* in *db/db* diabetic and *db/+* normoglycemic mice. There were six mice per group. Real-time PCR was carried out and the results from three different assays combined. Each value represents the mRNA level of the diabetic divided by the normoglycemic (means ± SE). For comparison, the corresponding values obtained by microarray analysis are presented as the means ± range as described in Tables 1–3.

hematoxylin and eosin. Van Gieson–stained sections described above were also used to measure newly formed bone, which is stained blue, whereas previously formed bone is stained red. The area of new bone formation area per bone length (mm^2/mm) was determined at 400× magnification by image analysis software. The length of eroded bone surface on day 8 was measured at 400× magnification in sections stained with hematoxylin and eosin as previously described (27), using an image analysis system. As an indication of the degree of coupling between bone formation and resorption, the amount of newly formed bone was divided by the percent eroded bone surface.

RNase protection assay. Total RNA was extracted from the scalps of mice using Trizol (Invitrogen, Rockville, MD). RNA from six animals was pooled, and gene expression was measured by a RNase protection assay. ^{32}P-labeled riboprobes specific for murine procollagen I and III were incubated with 4 μg total RNA. After hybridization, specimens were subjected to RNase digestion using a kit from BD Pharmingen (Franklin Lakes, NJ), following the manufacturer's instructions. After electrophoresis on a 6% polyacrylamide gel, radiolabeled bands were visualized using a PhosphorImager (Bio-Rad Laboratories, Hercules, CA). The optical density of the protected bands was measured with Image ProPlus software (Media Cybernetics, Silver Spring, MD), which was then normalized by the value of GAPDH (glyceraldehyde-3-phosphate dehydrogenase) in the same line. The results of three separate RNase protection assays were combined. Significance was determined by Student's *t* test.

Caspase activity. Caspase activity was assayed by a fluorometric kit purchased from R&D Systems (Minneapolis, MN). Frozen tissues from six specimens were pooled per data point, pulverized, and incubated in cell lysis buffer provided by R&D Systems. Total protein was determined using a BCA protein assay kit (Pierce, Rockford, IL). Then, ~300 μg of total protein was assayed per data point. Caspase-3 activity was detected, using the specific caspase-3 fluorogenic substrate DEVD [Z-Asp(OMe)-Glu(OMe)-Val-DL-Asp (OMe)] peptide conjugated to 7-amino-4-trifluoromethyl coumarin (AFC). Caspase-8 activity was detected by using the fluorogenic substrate, IETD [Z-Ile-Glu(OMe)-Thr-Asp(OMe)]-AFC and caspase-9 activity with LEHD [Z-Leu-Glu(OMe)-His-Asp(OMe)]-AFC. Measurements were made on a fluorescent microplate reader using filters for excitation (400 nm) and detection of emitted light (505 nm). The results of three separate assays were combined. Statistical difference between samples was determined by Student's *t* test.

RESULTS

To measure the impact of diabetes on healing of a bacteria-induced injury, bacteria were inoculated at the midline of the scalp between the ears of the mouse. This model facilitates quantitative analysis of both soft and hard tissue repair, apoptosis, and apoptosis pathways (22,23,28). To establish how diabetes modulates mRNA levels of apoptotic genes, RNA profiling was undertaken and the data analyzed by PathwayAssist software (Tables 1–3). A fairly conservative approach was taken in defining an increase as a minimum of 1.7-fold in each of two microarrays and at least 2.0-fold for the mean of the two arrays. Of the 276 total number of apoptotic genes identified by the software, mRNA levels of 71 were enhanced by diabetes, and 3 were downregulated. Of the 71 genes that increased twofold in diabetic specimens, 63 were proapoptotic, and 8 were antiapoptotic. Thus, diabetes had a global effect that was markedly proapoptotic. Apoptotic genes were subclassified into groups based on functional criteria: *1*) directly pro- or antiapoptotic, which includes mitochondrial factors and caspases; *2*) intercellular mediators, such as death-inducing ligands; *3*) receptors and intracellular mediators that include death receptors and accessory molecules; and *4*) transcription factors. Diabetes increased the RNA levels of genes in each of these categories, further supporting the impact of diabetes as altering the global pattern of apoptotic gene expression. Supplemental data in an online appendix (available at http://diabetes.diabetesjournals.org) provides a list of genes that were not modulated twofold.

Real-time PCR was carried out to verify diabetes-modulated RNA levels of TNF-α, caspase-3, caspase-9, FAS, FADD, and FOXO1 (Fig. 1). In every case where expression was enhanced by diabetes more than twofold in the microarray, real-time PCR confirmed the increase. For FOXO1, where the microarray data indicated less than a twofold increase, a similar result was obtained with real-time PCR.

To establish whether caspase activity was increased in diabetic mice at the functional level, protein was isolated from the healing tissue on days 5 and 8. We previously reported that initial healing takes place on day 5 and peaks on day 8, and the highest levels of apoptosis are found on day 8 (23). On day 5 the level of caspase-3, -8, and -9 activity was 2.2-, 2.5-, and 2.7-fold higher, respectively, in the diabetic compared with normoglycemic mice, all of which were significant ($P < 0.05$) (Fig. 2). On day 8 there was a 3-fold increase in caspase-3 activity, a 1.3-fold increase in caspase-8 activity, and a 1.9-fold higher level of caspase-9 activity in the diabetic mice. The difference between control and diabetic mice was statistically significant for each caspase tested ($P < 0.05$).

To assess the impact of enhanced caspase activity, diabetic mice were treated with a pancaspase inhibitor. The inhibitor was started 3 days after inoculation of bacteria to minimize the impact on the inflammatory response, which peaks 1 day after inoculation (23). The effect on fibroblast apoptosis was assessed in histological

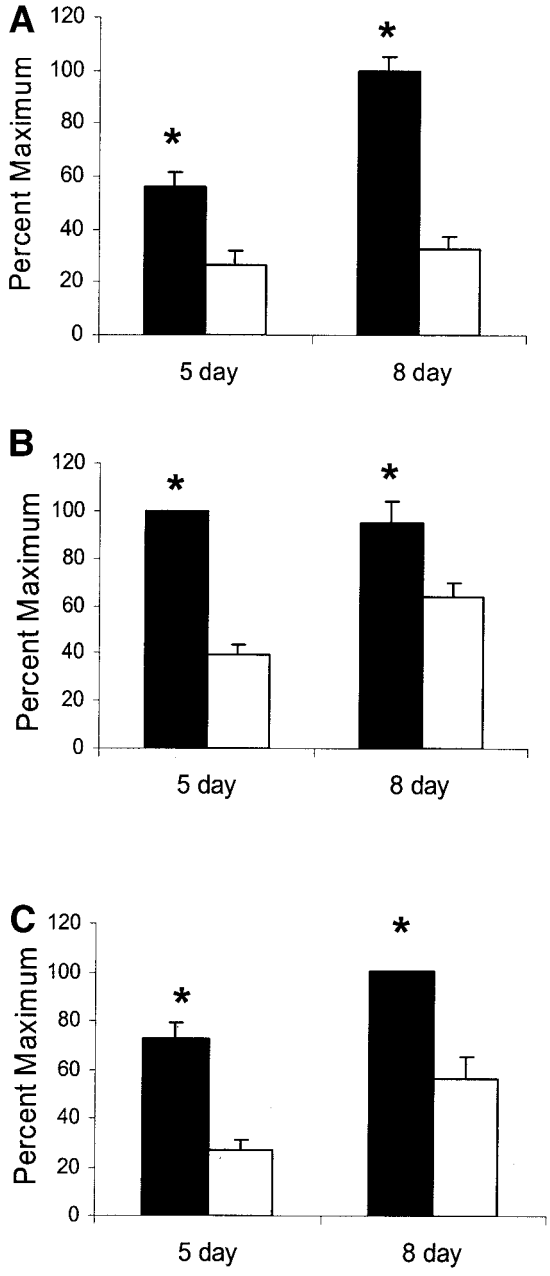

FIG. 2. Diabetes increases caspase-3 (*A*), caspase-8 (*B*), and caspase-9 (*C*) activities. Mice were inoculated with bacteria, and total protein was isolated 5 and 8 days later. Caspase activity was measured with a fluorometric kit. Each experiment was carried out three times, and the results were combined to give the means ± SE. *Significant difference between diabetic and diabetic mice treated with inhibitor ($P < 0.05$). ■, diabetic; □, control.

sections and identified by the characteristic appearance of fibroblasts in the TUNEL assay (Fig. 3). Quantitative analysis indicated that after the administration of caspase inhibitor, the number of apoptotic fibroblasts in the diabetic mice decreased only slightly on day 5 but was reduced by more than half on day 8, which was significant ($P < 0.05$) (Fig. 3*A*). The number of apoptotic fibroblasts was approximately sevenfold higher than that observed for leukocytes on days 5 and 8, indicating that the leukocytes represent a small percentage of apoptotic cells during healing (data not shown). Moreover, there was no difference in the number of apoptotic leukocytes in diabetic and normoglycemic mice (data not shown).

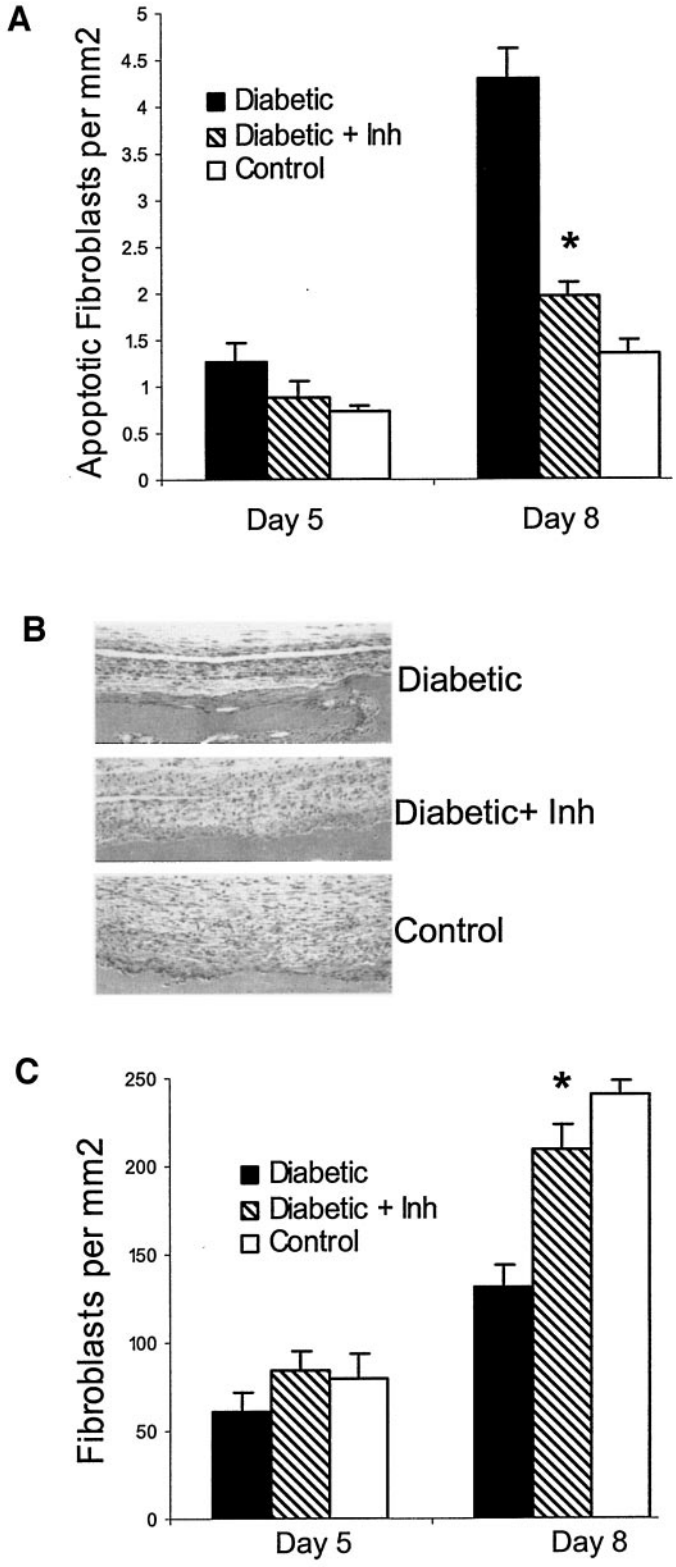

FIG. 3. Caspase inhibitor (Inh) reduces fibroblast apoptosis and increases fibroblast density in diabetic mice during the healing response to bacteria-induced injury. Bacteria were inoculated into the scalp of diabetic mice, diabetic mice treated with pancaspase inhibitor, or normoglycemic mice. There were six mice per data point ($n = 6$), and mice were killed on day 5 or 8. *A*: Quantitative analysis of TUNEL-positive fibroblastic cells *B*: Representative hematoxylin- and eosin-stained sections from specimens 8 days after bacterial inoculation. *C*: Quantitative analysis of fibroblast numbers. For *A* and *C*, each value represents the means ± SE. *Significant difference between diabetic mice and diabetic mice treated with inhibitor ($P < 0.05$).

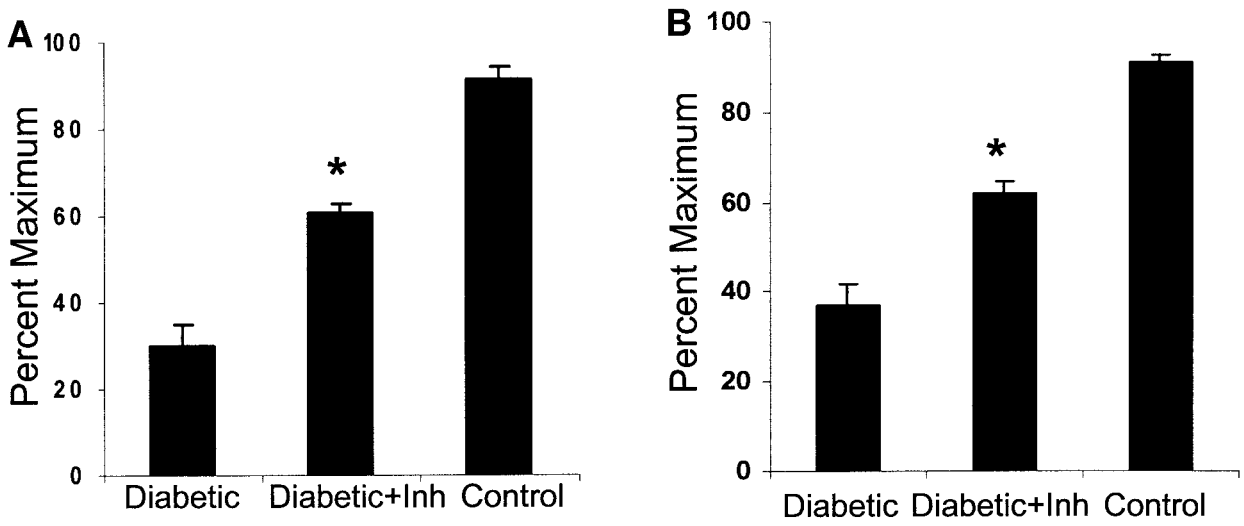

FIG. 4. Collagen mRNA expression is increased in diabetic mice after treatment with caspase inhibitor (Inh). Bacteria were inoculated into diabetic mice, diabetic mice treated with caspase inhibitor, and normoglycemic controls. Mice were killed 8 days after bacterial inoculation. There were six mice per group ($n = 6$). Procollagen I (*A*) and III (*B*) mRNA levels were measured by the RNase protection assay. The densitometric values of procollagen I and III were normalized by GAPDH (glyceraldehyde-3-phosphate dehydrogenase) levels in the same lane. Each assay was carried out three times and the values combined to give the means ± SE. *Significant difference between diabetic and diabetic mice treated with inhibitor ($P < 0.05$).

The potential impact of apoptosis on fibroblast numbers was measured in diabetic mice treated with caspase inhibitor compared with vehicle alone. Treatment with inhibitor substantially increased the number of fibroblasts (Fig. 3*B*). Quantitative analysis indicated that treatment with the caspase inhibitor did not increase fibroblast density on day 5 ($P > 0.05$). On day 8 there was a 1.6-fold increase, which was significant ($P < 0.05$). Moreover, fibroblast density in the diabetic group reached a level similar to that of normoglycemic animals ($P > 0.05$).

The formation of new matrix is a critical step in wound repair. The functional effect of diabetes-enhanced caspase-3 activity was measured by assessing the expression of procollagen I and III mRNA (Fig. 4). Treatment with caspase inhibitor increased expression of procollagen I by 2-fold and procollagen III by 1.7-fold, both of which were statistically significant ($P < 0.01$). Thus, treatment of diabetic mice with caspase inhibitor significantly enhanced collagen I and III mRNA to a level that was ~60% of the normoglycemic mice.

The formation of new connective tissue matrix was identified by VanGieson staining of histological sections (Fig. 5*A*). Treatment with caspase inhibitor improved the formation of extracellular matrix. The amount of new matrix produced in mice treated with caspase inhibitor was twofold higher than in the untreated mice, which was statistically significant and which agreed well with the increase in collagen expression ($P < 0.01$) (Fig. 5*B*). With caspase inhibitor the formation of new matrix was 69% of the value for normoglycemic controls, compared with 33% for the untreated diabetic mice.

In addition to examining changes in soft connective tissue, the calvarial model can be used to measure the impact of diabetes and apoptosis on new bone formation. In this model, a stimulus induces a cycle of bone resorption followed by repair (22,29). Recently formed bone was

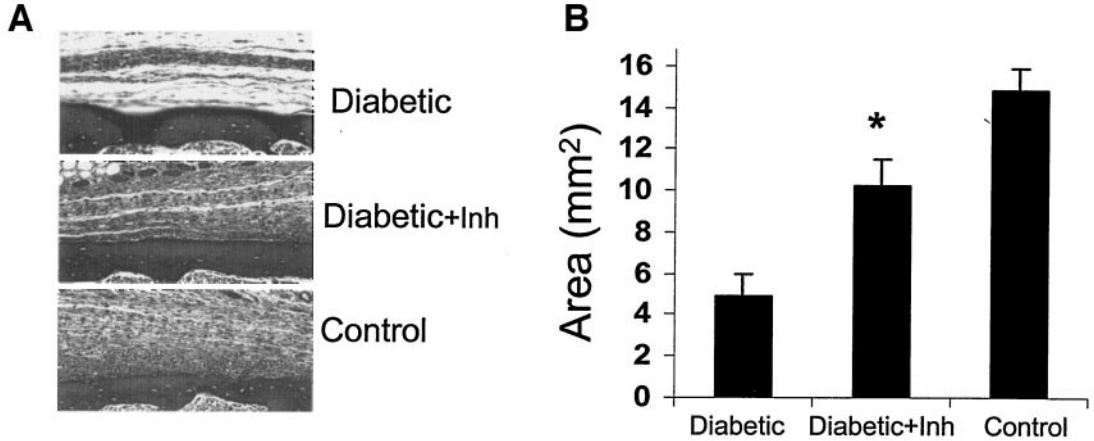

FIG. 5. Inhibition of caspase activity increases new connective tissue matrix formation in diabetic mice. Bacteria were inoculated into the scalp of diabetic mice, diabetic mice treated with pancaspase inhibitor (Inh), and normoglycemic controls. There were six mice per group ($n = 6$). Mice were killed 8 days after bacterial inoculation. *A*: Newly formed connective tissue matrix was identified in Van Gieson–stained histological sections by its characteristic blue color (original magnification 400×). *B*: The area of newly formed matrix on day 8 was measured with computer-assisted image analysis. Each value represents the means ± SE. *Significant difference between diabetic mice and diabetic mice treated with inhibitor ($P < 0.05$).

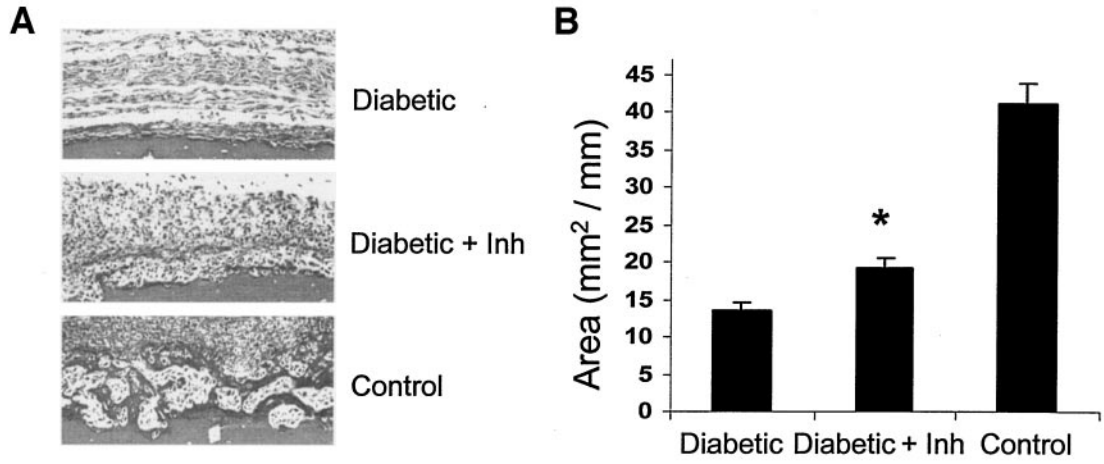

FIG. 6. Inhibition of caspase activity enhances new bone formation in diabetic mice. Bacteria were inoculated into the scalp of mice as described in Fig. 6. Mice were killed 8 days after bacterial inoculation. *A*: Newly formed bone matrix was identified in Van Gieson–stained sections by its characteristic blue color (original magnification 400×). *B*: The area of newly formed bone divided by the length of bone was measured with computer-assisted image analysis. Each value represents the means ± SE. *Significant difference between diabetic and diabetic mice treated with inhibitor ($P < 0.05$). Inh, caspase inhibitor.

identified by VanGieson staining (Fig. 6*A*). Histomorphometric analysis demonstrated that there was a 1.4-fold increase in bone formation in the diabetic mice treated with caspase blocker compared those treated with vehicle alone ($P < 0.01$) (Fig. 6*B*).

Both physiological and pathological bone remodeling involves a cycle of bone loss followed by bone formation. To assess this coupling phenomenon, the amount of newly formed bone was divided by a measure of bone loss, the percent eroded bone surface (Fig. 7). Diabetes caused a significant degree of uncoupling because the amount of bone formed per eroded bone surface was threefold less in the diabetic compared with normoglycemic mice ($P < 0.01$). Treatment with the caspase inhibitor significantly improved coupling by 1.4-fold, consistent with the degree of improvement in new bone formation ($P < 0.01$).

DISCUSSION

In the scalp/calvarial model, fixed bacteria are inoculated that induce an inflammatory injury, which is similar in normal and diabetic mice (23). We used fixed bacteria so that differences between diabetic and normoglycemic mice reflect differences in the host healing response rather than a diminished capacity of diabetic mice to kill bacteria. In this model soft and hard tissue healing occurs in a similar time frame, and the wound is not exposed to the outside environment where healing can be affected by external factors (22,23). Using this model we previously reported that diabetes causes an increase in apoptosis of critical matrix-producing cells (22,23). The current studies established that diabetes-enhanced apoptosis represents a physiologically important event by using a caspase inhibitor. Several parameters of healing were improved by blocking apoptosis. These included fibroblast density, level of collagen expression, and the amount of new connective tissue matrix formed. Treatment with caspase inhibitor significantly increased new bone formation as well, although the magnitude of the effect was less than that observed for soft connective tissue formation. Thus, the higher levels of diabetes-associated apoptosis of fibroblastic and osteoblastic cells previously reported (22,23) significantly contributes to a deficient healing response in diabetic individuals.

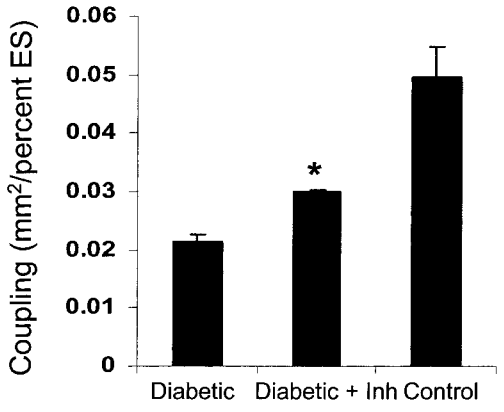

FIG. 7. Inhibition of caspase activity significantly improves bone coupling in diabetic mice. Bacteria were inoculated into the scalp of mice as described in Fig. 6, which were killed 8 days later. There were six mice per group ($n = 6$). The area of newly formed bone was divided by the percent eroded bone surface, a measure of bone resorption. Each value represents the means ± SE. *Significant difference between diabetic mice and diabetic mice treated with inhibitor ($P < 0.05$). ES, eroded surface; Inh, caspase inhibitor.

mRNA profiling experiments provided insight into mechanisms by establishing that diabetes caused a global induction of proapoptotic genes during the repair process. Of a total of 276 apoptotic genes examined, 71 genes increased twofold or more. Of these genes, 63 were proapoptotic and 8 were antiapoptotic genes. Only three genes were downregulated, and all of these were antiapoptotic. Although there have been no publications on the impact of diabetes on the global pattern of apoptotic gene expression during healing or in response to infection, it has been reported that diabetes enhances proapoptotic gene expression in the liver and retina of diabetic animals compared with normoglycemic animals (30,31). Thus, one of the potential mechanisms whereby diabetes negatively affects the function of an organ is to enhance the expression of proapoptotic genes. This, in turn, may promote apoptosis by tipping the intracellular balance in a proapoptotic direction.

One of the apoptotic genes upregulated at the RNA level was caspase-3. Functional studies indicated that caspase-3

activity was also enhanced in the diabetic group, along with both caspase-8 and caspase-9, suggesting that both extrinsic and intrinsic apoptotic pathways are involved. Activation of caspase-3 is associated with hyperglycemia-induced myocardial apoptosis (32) and apoptosis of neuronal cells in diabetic neuropathy (33–35). It is also associated with apoptosis of mesangial cells that occurs in diabetic nephropathy (36,37). Activation of caspase-3 typically occurs via the cytosolic and/or mitochondrial pathways (38). Data reported here indicate that both of these pathways appear to contribute to diabetes-enhanced apoptosis during dermal healing.

Previous studies have supported the concept that repopulation of wounds by fibroblasts is caused by a decrease in growth factor production and cellular proliferation (7,9). Thus, the failure to achieve a sufficient number of fibroblasts could potentially come from two different mechanisms: a failure to stimulate sufficient proliferation or a significantly enhanced rate of programmed cell death. Consistent with this principle are findings that conditions that enhance apoptosis are associated with impaired healing (39), whereas those that reduce apoptosis are correlated with qualitative and quantitative improvements in wound repair (40). Similarly, enhanced osteoblast apoptosis is thought to play a role in deficient bone formation. For example, glucocorticoid-induced osteoporosis occurs under conditions that enhance osteoblast apoptosis (41). Increased osteoblast apoptosis also impairs bone formation in myeloma bone disease (42). Conversely, reduced osteoblast apoptosis may enhance bone formation (43,44).

Therefore, studies presented here provide the first direct evidence that increased apoptosis of fibroblasts and osteoblasts caused by diabetes functionally contributes to impaired healing.

ACKNOWLEDGMENTS

This work was supported by National Institute of Dental and Craniofacial Research Grants DE07559 and DE11254.

We thank Renee Cabral for technical assistance and Alicia Ruff for help in preparing the manuscript.

REFERENCES

1. Engelgau M, Geiss MLS, Saaddine JB, Boyle JP, Benjamin SM, Gregg EW, Tierney EF, Rios-Burrows N, Mokdad AH, Ford ES, Imperatore G, Narayan KM: The evolving diabetes burden in the United States. *Ann Intern Med* 140:945–950, 2004
2. Coursin DB, Connery LE, Ketzler JT: Perioperative diabetic and hyperglycemic management issues. *Crit Care Med* 32:S116–S125, 2004
3. Rosenberg CS: Wound healing in the patient with diabetes mellitus. *Nurs Clin North Am* 25:247–261, 1990
4. Singh N, Armstrong DG, Lipsky BA: Preventing foot ulcers in patients with diabetes. *JAMA* 293:217–228, 2005
5. Pound N, Chipchase S, Treece K, Game F, Jeffcoate W: Ulcer-free survival following management of foot ulcers in diabetes. *Diabet Med* 22:1306–1309, 2005
6. American Diabetes Association: Consensus Development Conference on Diabetic Foot Wound Care: 7–8 April 1999, Boston, Massachusetts. *Diabetes Care* 22:1354–1360, 1999
7. Goodson WH 3rd, Hung TK: Studies of wound healing in experimental diabetes mellitus. *J Surg Res* 22:221–227, 1977
8. Bennett SP, Griffiths GD, Schor AM, Leese GP, Schor SL: Growth factors in the treatment of diabetic foot ulcers. *Br J Surg* 90:133–146, 2003
9. Hehenberger K, Hansson A, Heilborn JD, Abdel-Halim SM, Ostensson CG, Brismar K: Impaired proliferation and increased L-lactate production of dermal fibroblasts in the GK-rat, a spontaneous model of non-insulin dependent diabetes mellitus. *Wound Repair Regen* 7:65–71, 1999
10. Mansbridge JN, Liu K, Pinney RE, Patch R, Ratcliffe A, Naughton GK: Growth factors secreted by fibroblasts: role in healing diabetic foot ulcers. *Diabetes Obes Metab* 1:265–279, 1999
11. Rosenbloom AL, Silverstein JH: Connective tissue and joint disease in diabetes mellitus. *Endocrinol Metab Clin North Am* 25:473–483, 1996
12. Goova MT, Li J, Kislinger T, Qu W, Lu Y, Bucciarelli LG, Nowygrod S, Wolf BM, Caliste X, Yan SF, Stern DM, Schmidt AM: Blockade of receptor for advanced glycation end-products restores effective wound healing in diabetic mice. *Am J Pathol* 159:513–512, 2001
13. Darby IA, Bisucci T, Hewitson TD, MacLellan DG: Apoptosis is increased in a model of diabetes-impaired wound healing in genetically diabetic mice. *Int J Biochem Cell Biol* 29:191–200, 1997
14. Herskind AM, Christensen K, Norgaard-Andersen K, Andersen JF: Diabetes mellitus and healing of closed fractures. *Diabetes Metab* 18:63–64, 1992
15. Pietschmann P, Schernthaner G, Woloszczuk W: Serum osteocalcin levels in diabetes mellitus: analysis of the type of diabetes and microvascular complications. *Diabetologia* 31:892–895, 1988
16. Hou JC, Zernicke RF, Barnard RJ: Experimental diabetes, insulin treatment, and femoral neck morphology and biomechanics in rats. *Clin Orthop Relat Res* 278–285, 1991
17. Verhaeghe J, Suiker AM, Einhorn TA, Geusens P, Visser WJ, Van Herck E, Van Bree R, Magitsky S, Bouillon R: Brittle bones in spontaneously diabetic female rats cannot be predicted by bone mineral measurements: studies in diabetic and ovariectomized rats. *J Bone Miner Res* 9:1657–1667, 1994
18. Macey LR, Kana SM, Jingushi S, Terek RM, Borretos J, Bolander ME: Defects of early fracture-healing in experimental diabetes. *J Bone Joint Surg Am* 71:722–733, 1989
19. Strotmeyer ES, Cauley JA, Schwartz AV, Nevitt MC, Resnick HE, Bauer DC, Tylavsky FA, de Rekeneire N, Harris TB, Newman AB: Nontraumatic fracture risk with diabetes mellitus and impaired fasting glucose in older white and black adults: the health, aging, and body composition study. *Arch Intern Med* 165:1612–1617, 2005
20. de Liefde II, van der Klift M, de Laet CE, van Daele PL, Hofman A, Pols HA: Bone mineral density and fracture risk in type-2 diabetes mellitus: the Rotterdam Study. *Osteoporos Int* 16:1713–1720, 2005
21. Keegan TH, Schwartz AV, Bauer DC, Sellmeyer DE, Kelsey JL, the Fracture Intervention Trial: Effect of alendronate on bone mineral density and biochemical markers of bone turnover in type 2 diabetic women: the Fracture Intervention Trial. *Diabetes Care* 27:1547–1553, 2004
22. He H, Liu R, Desta T, Leone C, Gerstenfeld LC, Graves DT: Diabetes causes decreased osteoclastogenesis, reduced bone formation, and enhanced apoptosis of osteoblastic cells in bacteria stimulated bone loss. *Endocrinology* 145:447–452, 2004
23. Liu R, Desta T, He H, Graves DT: Diabetes alters the response to bacteria by enhancing fibroblast apoptosis. *Endocrinology* 145:2997–3003, 2004
24. Holt SC, Ebersole J, Felton J, Brunsvold M, Kornman KS: Implantation of *Bacteroides gingivalis* in nonhuman primates initiates progression of periodontitis. *Science* 239:55–57, 1988
25. Graves D, Jiang Y, Genco C: Bacterial virulence factors host response and impact on systemic health. *Curr Opin Infect Dis* 13:227–232, 2000
26. Bancroft J, Cook H: *Manual of Histological Techniques*. Edinburgh, Scotland, U.K., Nuttall Publishing, 1995
27. Parfitt AM: Bone histomorphometry: proposed system for standardization of nomenclature, symbols, and units. *Calcif Tissue Int* 42:284–286, 1988
28. Alikhani M, Alikhani Z, He H, Liu R, Popek BI, Graves DT: Lipopolysaccharides indirectly stimulate apoptosis and global induction of apoptotic genes in fibroblasts. *J Biol Chem* 278:52901–52908, 2003
29. Uy HL, Mundy GR, Boyce BF, Story BM, Dunstan CR, Yin JJ, Roodman GD, Guise TA: Tumor necrosis factor enhances parathyroid hormone-related protein-induced hypercalcemia and bone resorption without inhibiting bone formation in vivo. *Cancer Res* 57:3194–3199, 1997
30. Dhahbi JM, Mote PL, Cao SX, Spindler SR: Hepatic gene expression profiling of streptozotocin-induced diabetes. *Diabetes Technol Ther* 5:411–420, 2003
31. Joussen AM, Huang S, Poulaki V, Camphausen K, Beecken WD, Kirchhof B, Adamis AP: In vivo retinal gene expression in early diabetes. *Invest Ophthalmol Vis Sci* 42:3047–3057, 2001
32. Cai J, Ahmad S, Jiang WG, Huang J, Kontos CD, Boulton M, Ahmed A: Activation of vascular endothelial growth factor receptor-1 sustains angiogenesis and Bcl-2 expression via the phosphatidylinositol 3-kinase pathway in endothelial cells. *Diabetes* 52:2959–2968, 2003
33. Schmeichel AM, Schmelzer JD, Low PA: Oxidative injury and apoptosis of dorsal root ganglion neurons in chronic experimental diabetic neuropathy. *Diabetes* 52:165–171, 2003
34. Low P, Schmeichel A, Schmelzer J, Kishi M: Oxidative stress in the pathogenesis of experimental diabetic neuropathy. *J Neurochem* 85 (Suppl. 2):14, 2003
35. Li Z, Zhang W, Grunberger G, Sima A: Hippocampal neuronal apoptosis

intype 1 diabetes. *Brain Res* 946:221–231, 2002
36. Lee HB, Ha H: Development and progression of diabetic nephropathy: future interventions (Review). *Pol Arch Med Wewn* 102:19–27, 1999
37. Yamagishi S, Amano S, Inagaki Y, Okamoto T, Takeuchi M, Makita Z: Beraprost sodium, a prostaglandin I2 analogue, protects against advanced glycation end products-induced injury in cultured retinal pericytes. *Mol Med* 8:546–550, 2002
38. Earnshaw WC, Martins LM, Kaufmann SH: Mammalian caspases: structure, activation, substrates, and functions during apoptosis. *Annu Rev Biochem* 68:383–424, 1999
39. Qu J, Cheng T, Shi C, Lin Y, Yan G, Ran X: Reduced presence of tissue-repairing cells in wounds combined with whole-body irradiation injury is associated with both suppression of proliferation and increased apoptosis. *Med Sci Monit* 9:BR370–BR377, 2003
40. Ono I, Yamashita T, Hida T, Jin HY, Ito Y, Hamada H, Akasaka Y, Ishii T, Jimbow K: Local administration of hepatocyte growth factor gene enhances the regeneration of dermis in acute incisional wounds. *J Surg Res* 120:47–55, 2004
41. Weinstein RS, Jilka RL, Parfitt AM, Manolagas SC: Inhibition of osteoblastogenesis and promotion of apoptosis of osteoblasts and osteocytes by glucocorticoids: potential mechanisms of their deleterious effects on bone. *J Clin Invest* 102:274–282, 1998
42. Silvestris F, Cafforio P, Calvani N, Dammacco F: Impaired osteoblastogenesis in myeloma bone disease: role of upregulated apoptosis by cytokines and malignant plasma cells. *Br J Haematol* 126:475–486, 2004
43. Stanislaus D, Yang X, Liang JD, Wolfe J, Cain RL, Onyia JE, Falla N, Marder P, Bidwell JP, Queener SW, Hock JM: In vivo regulation of apoptosis in metaphyseal trabecular bone of young rats by synthetic human parathyroid hormone (1–34) fragment. *Bone* 27:209–218, 2000
44. Jilka RL, Weinstein RS, Bellido T, Roberson P, Parfitt AM, Manolagas SC: Increased bone formation by prevention of osteoblast apoptosis with parathyroid hormone. *J Clin Invest* 104:439–446, 1999